Proceedings of ASME Turbo Expo 2011
GT2011
June 6-10, 2011, Vancouver, British Columbia, Canada

GT2011-45621

TRANSITION MODELLING FOR VORTEX GENERATING JETS ON LOW-PRESSURE TURBINE PROFILES

Florian Herbst [*]
Institute of Turbomachinery and Fluid Dynamics
Leibniz Universität Hannover
Hannover, 30167
Germany
Email: Herbst@tfd.uni-hannover.de

Dragan Kožulović
Institute of Fluid Mechanics
Technische Universität Braunschweig
Braunschweig, 38106
Germany
D.Kozulovic@tu-braunschweig.de

Joerg R. Seume
Institute of Turbomachinery and Fluid Dynamics
Leibniz Universität Hannover
Hannover, 30167
Germany
Email: Seume@tfd.uni-hannover.de

ABSTRACT

Steady blowing vortex generating jets (VGJ) on highly-loaded low-pressure turbine profiles have shown to be a promising way to decrease total pressure losses at low Reynolds-numbers by reducing laminar separation. In the present paper, the state of the art turbomachinery design code TRACE with RANS turbulence closure and coupled γ-Re_Θ transition model is applied to the prediction of typical aerodynamic design parameters of various VGJ configurations in steady simulations. High-speed cascade wind tunnel experiments for a wide range of Reynolds-numbers, two VGJ positions, and three jet blowing ratios are used for validation. Since the original transition model overpredicts separation and losses at $Re_{2is} \leq 100 \cdot 10^3$ an extra mode for VGJ induced transition is introduced. Whereas the criterion for transition is modelled by a filtered Q vortex criterion the transition development itself is modelled by a reduction of the local transition-onset momentum-thickness Reynolds number. The new model significantly improves the quality of the computational results by capturing the corresponding local transition process in a physically reasonable way. This is shown to yield an improved quantitative prediction of surface pressure distributions and total pressure losses.

NOMENCLATURE

B	=	blowing ratio, Eqn. (1)
c_p	=	pressure coefficient, $(p_x - p_1)/(p_{t,1} - p_1)$
c_{VGJ}	=	calibration coefficient
l	=	chord length
Ma	=	Mach number
n	=	wall normal coordinate
p	=	pressure
Q	=	vortex criterion, Eqn. (6)
Re	=	Reynolds number, $(U \cdot l_{ax} \cdot \rho)/\mu$
Re_Θ	=	momentum-thickness Reynolds number, $(U \cdot \Theta \cdot \rho)/\mu$
$\tilde{R}e_{\Theta t}$	=	local transition-onset Re_Θ from transport equation
S	=	strain-rate tensor, symmetric part of $\nabla\vec{U}$
t	=	pitch or wall tangential coordinate
U	=	magnitude of velocity
$\vec{U}$	=	velocity vector
x, y, z	=	Cartesian coordinates
y^*	=	distance to nearest wall
Zw	=	Zweifel no., Eqn. (16)

Greek

β	=	flow angle in x, y-plane (pitch)
γ	=	intermittency of transition model
δ	=	boundary layer thickness
ζ_V	=	total pressure loss, $(p_{t,1} - p_{t,2})/(p_{t,1} - p_1)$
Θ	=	momentum thickness
θ	=	VGJ skew angle

[*]Address all correspondence to this author.

μ = dynamic viscosity
μ_t = eddy viscosity
ρ = density
τ_w = wall shear stress
ϕ = VGJ pitch angle
Ω = vorticity tensor, asymmetric part of $\nabla\vec{U}$
$\vec{\omega}$ = vorticity vector, $\nabla\times\vec{U}$

Subscripts

ax in axial direction
is isentropic
jet value of the jet
m conservative average
rel relative
t total flow condition or transition onset
1 inlet
2 $0.4\cdot l_{ax}$ downstream trailing edge
∞ outer flow

Abbreviations

AFC active flow control
BL boundary layer
CFD computational fluid dynamics
DLR German Aerospace Centre
DNS direct numerical simulations
JICF jet in crossflow
LES large eddy simulations
LPT low-pressure turbine
PS pressure side
RANS Reynolds-averaged Navier-Stokes
SS suction side
SST shear-stress transport
URANS unsteady RANS
VGJ vortex generating jet

INTRODUCTION

Laminar-turbulent transition plays a significant role in the boundary layer development on modern highly-loaded low-pressure turbine (LPT) profiles. Especially at Reynolds numbers below $Re_{2is} < 100\cdot10^3$ which typically occur at high altitude flight in aircraft engines these profiles are susceptible to high losses associated to laminar separation and turbulent reattachement of the boundary layer on their suction side's diffusive section [1, 2]. Since further increasing the blade loading by decreasing blade count and the number of stages is a promising way to reduce weight and costs of future LPTs, high-lift profiles with Zweifel numbers $Zw > 1$ gain more and more importance in their design [3]. For these profiles separation induced losses may increase up to 300% of their values at design point [4] which may significantly compromise the engines efficiency [5, 6].

This loss characteristic for decreasing *Re* can be traced back to a massive increase of the thickness and length of the separation bubble, potentially culminating in a non-reattachement of the boundary layer. In the latter case the turbulent fluctuations developing in the separated shear layer are not providing a sufficient level of crossflow mixing in order to increase the momentum of the recirculating zone's fluid. A way to elevate the mixing and to improve the laminar boundary layer's resistance to separation at adverse pressure gradients are passive and active flow control methods [7].

The effectiveness of separation control by passive methods on LPT profiles has been shown by several authors using various techniques. E.g. Lou et al. [8] investigated a spanwise groove on a highly-loaded PAK-B profile downstream the suction side's pressure minimum but upstream the separation point by applying large eddy simulations (LES). They showed that the groove is able to shorten and thin the separation bubble by moving the onset of transition upstream. Himmel et al. [9] experimentally investigated the impact of several discrete roughness elements and of a spanwise rectangular groove on the boundary layer of the T106 LPT profile for a wide range of *Re*. Whereas the groove caused a loss reduction for the whole *Re* range the roughness elements only reduced losses for low *Re* and introduced additional losses compared to the baseline case for high *Re* due to their blockage effect. This undesireable effect is typical for many passive devices on LPT profiles (e.g. see [10]) and foils the advantage of their simplicity.

Since active flow control (AFC) methods require the expenditure of additional energy [7] they certainly cause more effort than the passive methods. Nevertheless, in order to avoid undesired losses they offer the possibility to be optimized in strength with regard to the operating point or to be completely turned off. Among others (e.g. plasma acuators) vortex generating jets (VGJs) are investigated [4, 10–15] and show considerable reduction of the separation and the losses, respectively. Besides steadily blowing VGJs, which are subject of this work, especially pulsed blowing [6] and zero-massflow (synthetic) jets [16] are in the focus of AFC research as they have shown to be more effective than the steady ones. However, in contrast to other AFC devices the introduction of VGJs could particularly benefit from the longtime experience with film-cooling configurations for high-pressure turbine stages with regard to the constructional implementation in an actual aircraft engine.

Injecting fluid from small holes with a pitch angle of $\phi = 90°$ in a crossflow induces a flow structure well-known in literature as *jet in crossflow* (JICF) phenomenon [17]. Figure 1 illustrates the main vortices induced by a JICF: the dominating counter-rotating vortex pair (CVP) which is aligned with the jet trajectory as well as the secondary vortex structures like the horse-shoe vortex (HSV) on the surface around the jet, the wake vortices downstream the injection position, and the shear-layer vortices.

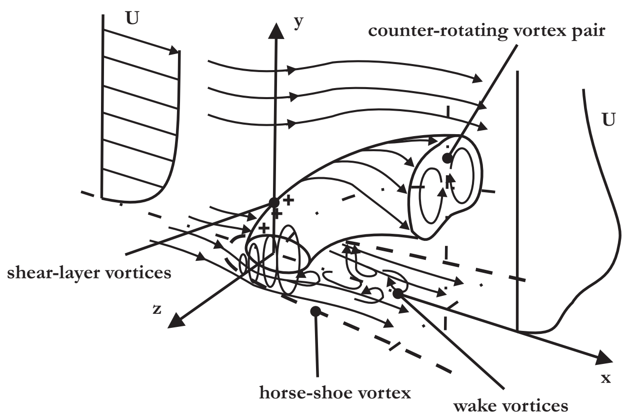

FIGURE 1. Vortex structures of a jet in crossflow configuration according to [17]

Especially the streamwise CVP has shown to be responsible for an improved mixing between the outer flow and the fluid close to the wall.

Basic investigations of Compton and Johnston [18] revealed that for blowing with a lower pitch angle $\phi = 45°$ and high skew angles $\theta = 45°...90°$ (between the streamwise direction and the blowing axis) a maximum of vorticity can be achieved, whereas the CVP gradually collapses to one dominant streamwise vortex for increasing θ [19]. Besides the injection angle the non-dimensional blowing ratio

$$B = \frac{(\rho U)_{jet}}{(\rho U)_{\infty}} \tag{1}$$

has a direct impact on the maximum vorticity [18] and hence, has to be considered as a basic VGJ design parameter. For an effective loss reduction a minimum B needs to be exceeded [4] which depends on the VGJs position [20]. Additionally, to the increased mixing by large-scale vortices the jet promotes transition to turbulence which reduces the tendency of the boundary layer to separation as well [21]. With regard to the VGJ's effectiveness direct numerical simulations (DNS) revealed that the interaction of large-scale vortices and the transition triggering effect strongly depends on B. Whereas at low B (<1) the separation is reduced by promoting transition, at high B the reduction is reached by large-scale vortices [13].

The numerous parameters illustrate that a design tool is required, which captures all the relevant flow features in order to design a LPT with VGJs correctly. Various authors (e.g. [13,22,23]) have published results of few selected configurations (and operating points) by using LES and DNS codes, capturing many flow features in detail and allowing valuable analysis of the underlying physics, respectively. Nevertheless, taking into account limited time and CPU resources as well as the state of the art, a RANS-code with a two-equation turbulence model is still industrial design tool of choice. In order to obtain reliable, quantitative results of the parameters relevant for design, the physical fidelity must be improved by more suitable modelling.

Simulations of experimental VGJ configurations using the SST turbulence model [24] revealed that although the disappearance of the separated region is well predicted the wake characteristics are not. Rumsey and Swanson [25] showed that current RANS-models (without an extra transition model) tend to underpredict turbulent eddy viscosity in the near-wall shear layers (e.g. found in separation bubbles and VGJs). Anyway, nowadays standard computational procedure for the simulation of LPT flows (without VGJs) of coupling a two-equation turbulence model (e.g. k-ω- or SST-model) with a correlation-based transition model successfully addresses this problem for separation-induced transition [26–28]. A previous systematic and comprehensive study applying RANS with and without additional non-local transition model to VGJ experiments of a high-speed cascade wind tunnel over a wide range of Re [15] showed the discrepancies of this approach. Especially at the relevant low Re ($<100 \cdot 10^3$) too high losses are predicted which can be traced back to a separation of the boundary layer downstream the VGJs. A similar study for pulsed blowing using the local γ-Re_θ transition model [27] and URANS confirms this results [6]. This characteristic is probably caused by an unrealistic too low eddy viscosity level.

In the current work this problem is addressed by the development of an extra half-empiric transition correlation for the γ-Re_θ model in order to capture VGJ induced transition effects for steady blowing. At first a local transition criterion is developed using a generic testcase. In the next step the development of the transition is modelled by a reduction of $\tilde{Re}_{\Theta t}$. The new model is validated against extensive wind tunnel experiments of a high-lift LPT profile for a wide range of Re, two VGJ positions, three blowing ratios at high speed conditions ($Ma_{2is} = 0.6$) and with an inlet freestream turbulence intensity of Tu_1 =4%.

NUMERICAL METHOD

The CFD simulations in the current work are performed with the turbomachinery research and design code TRACE which is developed by the German Aerospace Centre (DLR) [29]. TRACE solves the three-dimensional RANS equations on structured and unstructured multi-block meshes by a finite volume approach whereas convective fluxes are discretized by Roe's second-order accurate upwind scheme and diffusive fluxes by a central differencing scheme [26, 30]. Only steady computations are performed in this paper using an implicit second-order predictor corrector time integration. The RANS turbulence closure is modelled by a Wilcox implementation of the k-ω two-equation model [31] including the additional Kato-Launder stagnation point anomaly fix [32].

Throughout this paper the boundary layers of all no-slip boundaries are highly resolved with a dimensionless wall distance of the wall adjacent cell down to $n^+ = 1$. Convergence could be achieved for all cases presented here with a maximum density residual of at least $\leq 10^{-2}$ and a relative difference of in- and outlet massflow $\leq 10^{-3}$.

TRACE incorporates two correlation-based transition models which are linked to the k-ω-model: (1) The non-local *multimode transition model* evaluates integral boundary layer parameters in order to control the transition process. It has been calibrated to provide good results of natural, bypass, separation, and wake induced transition for typical turbomachinery configurations [26]. (2) The γ-Re_Θ transport equation transition model evaluates local flow features to model natural, bypass and separation induced transition [27]. Marciniak et al. [28] compared the *multimode model* to the TRACE implementation of the γ-Re_Θ model using alternative transition correlations of Malan et al. [33] (in the current work the correlations of Langtry and Menter [27] are applied). They showed by means of several turbomachinery test cases that only minor differences exist between both models which can be traced back to their calibration.

However, since a local evaluation of transition criteria is more appropriate for the complex, three dimensional flow of a jet in crossflow the γ-Re_Θ model is used throughout the current work. Hence, the transport equations for γ (Eqn. 2) and $\tilde{R}e_{\Theta t}$ (Eqn. 3) are the base for the development of the VGJ transition mode:

$$\frac{\partial(\rho\gamma)}{\partial t} + \frac{\partial(\rho U_i \gamma)}{\partial x_i} = P_\gamma - E_\gamma + \frac{\partial}{\partial x_i}\left[\left(\mu + \frac{\mu_t}{\sigma_f}\right)\frac{\partial \gamma}{\partial x_i}\right] \quad (2)$$

$$\frac{\partial(\rho \tilde{R}e_{\Theta t})}{\partial t} + \frac{\partial(\rho U_i \tilde{R}e_{\Theta t})}{\partial x_i} = P_{\Theta t} + \frac{\partial}{\partial x_i}\left[\sigma_{\Theta t}(\mu + \mu_t)\frac{\partial \tilde{R}e_{\Theta t}}{\partial x_i}\right]. \quad (3)$$

Whereas the production term P_γ and destruction term E_γ of the γ equation as well as the production term $P_{\Theta t}$ of the $Re_{\Theta t}$ incorporate the empirical transition correlations for natural and bypass transition. Separation induced transition is controlled by

$$\gamma_{eff} = \max(\gamma, \gamma_{sep}) \quad (4)$$

with

$$\gamma_{sep} = \min\left(s_1 \max\left[0, \frac{Re_\theta}{3.235 Re_{\theta_c}} - 1\right] F_{reattach}, 2\right) F_{\theta_t}. \quad (5)$$

For the complete description and the definitions of the coefficients mentioned in Eqn. (2) - (5) please see Langtry and Menter [27].

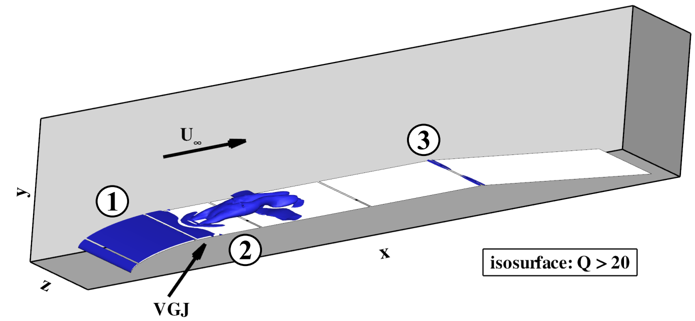

FIGURE 2. Q vortex criterion at VGJ flat plate setup

DERIVING THE MODEL
Transition Criterion

The DNS of Postl [13] showed that immediately downstream the injection position longitudinal vortices are induced in the crossflow by steady VGJs. These vortices decay initially, reappear downstream and breakdown to turbulence even further downstream as indicated by the formation of hairpin-vortices. Whereas the large-scale longitudinal vortices close to the injection position can be detected in steady RANS simulations (e.g. [15]) the last two stages of the transition process are scarcely captured by a two-equation eddy viscosity turbulence model. Thus, they must be the object of an adapted transition modelling with a direct change of γ or a modification of the production terms of the γ-Re_Θ transport equations. In order to apply these modifications at the correct positions in three-dimensional space a distinct indicator is needed. Since vortex detection criteria, e.g. the λ_2-criterion [34] or the Q-criterion [35], are able to visualize the vortical structures of VGJs (e.g. [13]), they are a convenient choice for such an indicator. Figure 2 shows the vortex cores as detected by

$$Q = \frac{1}{2}\left[|\Omega|^2 - |S|^2\right] > 20. \quad (6)$$

of a generic testcase which is used in the following for the development of the VGJ transition criterion.

The selected testcase consists of a flat plate with a pressure distribution similar to that of a high-lift LPT's suction side and is based on the experimental setup of Lengani et al. [36]. In order to ensure a sufficient high Ma for the density-based solver TRACE the geometry is scaled by a factor of 0.1 while keeping the Reynolds number constant. Figure 3 shows the configuration including a VGJ close to the pressure minimum. The

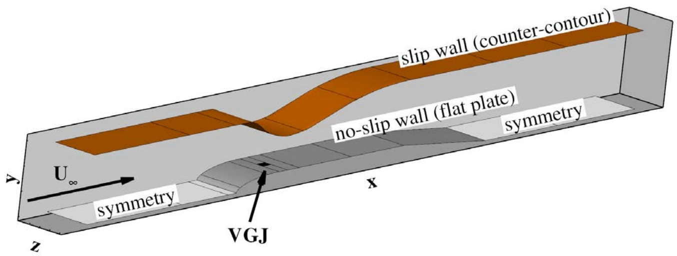

FIGURE 3. Flat plate setup with boundary conditions (translational-periodic boundary condition in z-direction)

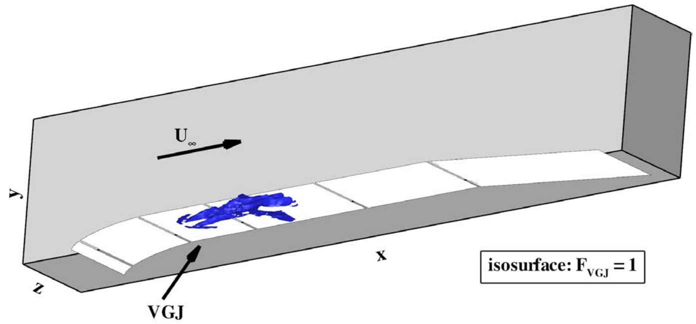

FIGURE 4. VGJ transition criterion F_{VGJ}

jet is injected with a blowing ratio of $B = 0.5$, an angle to the streamwise tangent at the plate surface (pitch angle) of $\phi = 45°$, and an angle between the streamwise direction and the blowing axis (skew angle) of $\theta = 0°$. The computations are performed at $Re_1 = 100 \cdot 10^3$ with an turbulence intensity of $Tu_1 = 0.01$.

In Fig. 2 three regions $Q > 20$ can be distinguished : ①Close to the surface at the flat plate's convex curved leading edge a thin Q-vortex layer is detected. This result is consistent to simulations of the LPT profile (which is used in the next section) where this kind of layer can also be observed especially on the profiles suction side (not shown here). ②The two dominant vortical structures of the JICF (Fig. 1) - the horse-shoe vortex upstream and around the injection position and the counter-rotating vortex pair downstream - are captured. ③At the sharp bend, close to the end of the plate's horizontal area two unconnected long and thin vortex cores normal to the streamwise direction are visible.

While the detection of region ② is a promising result as it indicates places where a manipulation of the transition model is reasonable, regions ① and ③ need to be excluded. This is achieved by filtering the Q criterion with the magnitude of the relative helicity (viz. the streamwise component of the vorticity vector)

$$\omega_{sw,rel} = \frac{\vec{U} \cdot \vec{\omega}}{|\vec{U}| \cdot |\vec{\omega}|}. \tag{7}$$

Applying this filter the VGJ transition criterion F_{VGJ} is derived by

$$F_{VGJ} = \begin{cases} 1, & \text{for: } f(Q, Arg_2, |\omega_{sw,rel}|) \\ 0, & \text{for: others.} \end{cases} \tag{8}$$

In order to ensure that the filter mainly captures the thin Q-layer close to the convex surface (region ①) it is basically applied in a subregion of the boundary layer close to the wall, which is defined by the component

$$Arg_2 = 1.0 - \left(\frac{\gamma - 1/c_{e2}}{1.0 - 1/c_{e2}} \right)^2 \tag{9}$$

of the $F_{\Theta t}$ blending function (Eqn. 12). Figure 4 shows the resulting 3D distribution of $F_{VGJ} = 1$ for the investigated testcase and Fig. 11 the corresponding result of a LPT profile with three VGJs. Due to the filtering only the streamwise vortical structures induced by the VGJ remain.

It is worth mentioning that the Q criterion as a specific function of S and Ω has been applied here to detect VGJ induced transition. But other combinations of S and Ω have been used by many other authors to model streamline curvature effects on turbulence development, e.g. used by Kožulović and Röber [37].

Transition Process

Postl's DNS [13] showed a significant streamwise gap between the primary longitudinal vortices and the onset of transition. In the current work this delay is taken into account by modifying $P_{\Theta t}$ which compared to the other possibilities offers a indirect, delayed approach to control transition. The original (unmodified) production term is given by

$$P_{\Theta t,orig} = c_{\Theta t}(Re_{\Theta t} - \tilde{R}e_{\Theta t})(1 - F_{\Theta t})\frac{\rho}{t^*} \tag{10}$$

with

$$t^* = \frac{500\mu}{\rho U^2}. \tag{11}$$

Due to the blending function $F_{\Theta t}$ (Eqn. 12) which equals 1 in the boundary layer and 0 outside $P_{\Theta t,orig}$ is only active in the free stream outside the boundary layer:

$$F_{\Theta t} = \min\left(\max\left(Arg_1, Arg_2\right), 1.0\right) \tag{12}$$

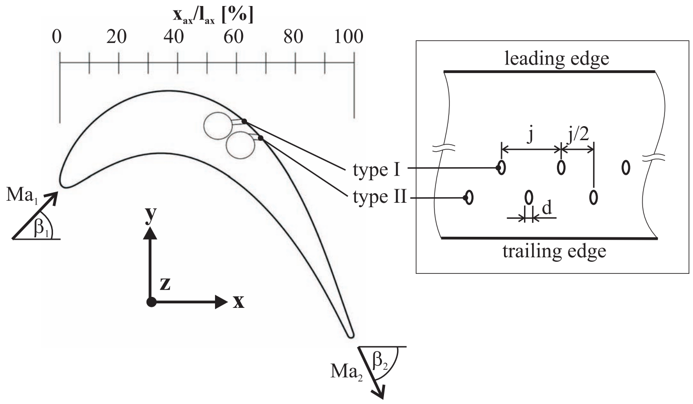

FIGURE 5. T161 high-lift LPT profile with two VGJ-configurations, type I at 63% and type II at 69% axial length, with $d/l_{ax} = 0.020$ and $j/d = 10$ (distorted geometry)

with

$$Arg_1 = F_{Wake} \cdot e^{\left(\frac{y^*}{\delta}\right)^4}. \tag{13}$$

Whereas this approach is convenient to model natural and especially bypass transition by the diffusion of $\tilde{R}e_{\Theta t}$ in the boundary layer it is not suitable for a VGJ transition mode. By inducing vortices in the boundary layer (especially at low B) the VGJ's impact on transition takes place in the near-wall region. Therefore, the contrary approach is selected here and the production term modification is limited on the boundary layer. Equation (14) gives the definition of the newly introduced production term

$$P_{\Theta t,VGJ} = c_{VGJ}(100 - \tilde{R}e_{\Theta t})F_{\Theta t}\frac{\rho}{t^*}. \tag{14}$$

The transitional effects are modelled by negative values of $P_{\Theta t,VGJ}$ which scale with the difference of the local $\tilde{R}e_{\Theta t}$ to its lower limit 100. Both production terms are combined by

$$P_{\Theta t,new} = F_{VGJ}P_{\Theta t,VGJ} + (1 - F_{VGJ})P_{\Theta t,orig}. \tag{15}$$

In the following figures all computations with the unmodified, original γ-Re_Θ model are referred to as *PDE-Transition*. Results of the newly introduced model are labelled as *PDE-Transition_VGJMod*.

VALIDATION

Testcase

For the validation, the highly loaded low-pressure turbine profile T161 described by Gier et al. [3] and investigated by Herbst et al. [15] is selected (Fig. 5). The T161 offers a high pitch ($t/l = 0.96$) and an aggressive suction side, resulting in a Zweifel number of

$$Zw = \frac{2t}{l_{ax}} \cos^2\beta_2(\tan\beta_2 + \tan\beta_1) = 1.14 \tag{16}$$

at design point. At low Re_{2is} ($\leq 120 \cdot 10^3$) it faces a strong increase in losses (Fig. 6 right) due to an increasing laminar separation bubble on its suction side: at $Re_{2is} = 200 \cdot 10^3$ the separation point is at around 80%, at $70 \cdot 10^3$ it is at around 75% axial length, turbulent reattachment takes place at around 90% in both operating points (see experimental values in Fig. 7). The heavily increasing losses for decreasing Re turn the T161 into a convenient object for AFC, with the aim to improve its performance at low Re and leave it uncontrolled at higher Re. Hence, the profile is equipped with two rows of VGJ upstream the suction side's separation point - the first row of nine holes at 63% (type I) and the second of ten holes at 69% axial length (type II). In both cases the jet's pitch angle is $\phi = 45°$ and its skew angle is $\theta = 0°$. Further jet properties are illustrated in Fig. 5.

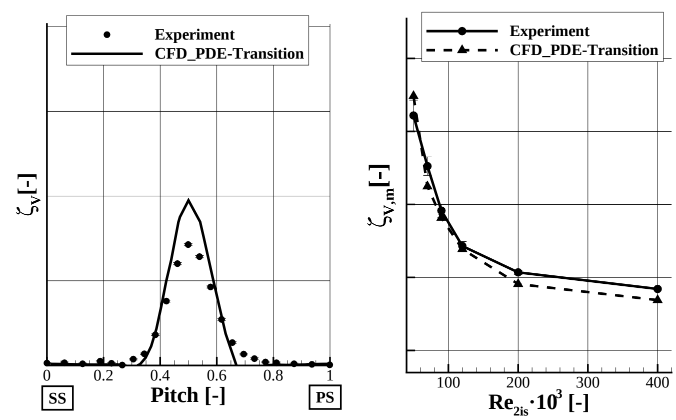

FIGURE 6. ζ_V of $Re_{2is} = 200 \cdot 10^3$ (left) and ζ_V, m for $Re_{2is} = 50 \cdot 10^3 ... 400 \cdot 10^3$ (right) without AFC

In extensive cascade wind tunnel experiments [38], surface pressure distributions c_p and wake losses ζ_V at $0.4 \cdot l_{ax}$ downstream the profile's trailing edge were measured. By applying the conservative averaging procedure of Amecke [39] the wake losses were reduced to $\zeta_{V,m}$. All experimental values are plotted with 98% confidence intervals. The experiments cover a range of isentropic outlet Reynolds numbers $Re_{2is} = 50 \cdot 10^3 ... 400 \cdot 10^3$

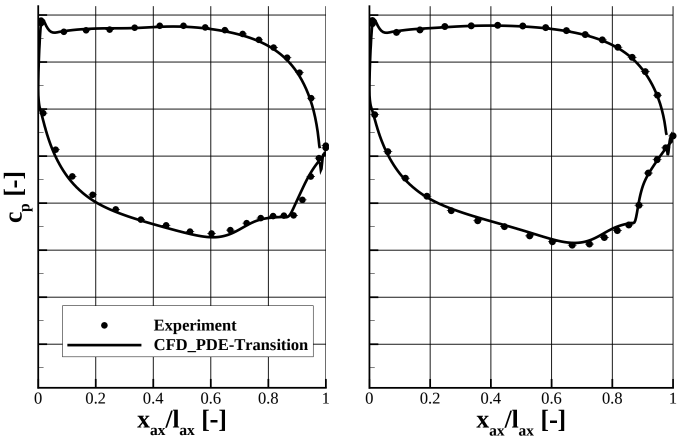

FIGURE 7. c_p of $Re_{2is} = 70 \cdot 10^3$ (left) and $200 \cdot 10^3$ (right) without AFC

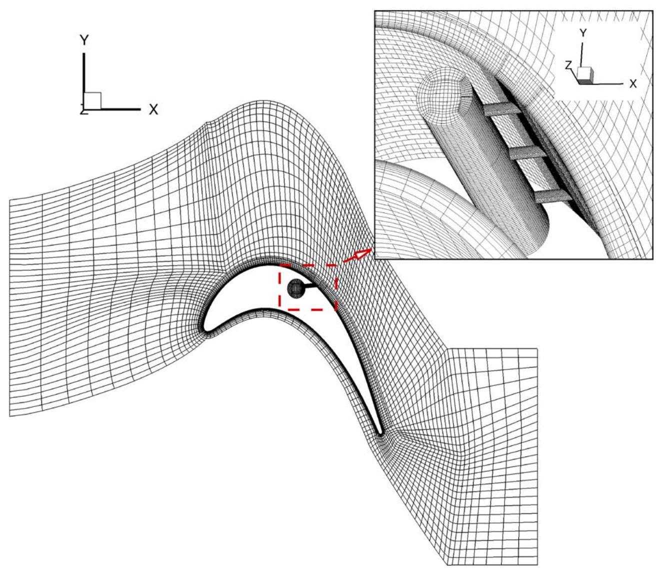

FIGURE 8. Mesh of type I VGJ, every second grid line shown (distorted geometry)

with an isentropic outlet Mach number of $Ma_{2is} = 0.6$ and an inlet turbulence intensity of $Tu_1 = 4\%$. Steady blowing ratios of $B = 0.5 \ldots 1.5$ were investigated.

Please note that the lowest $Re_{2is} = 50 \cdot 10^3$ at outlet corresponds to an $Re_1 \approx 30 \cdot 10^3$ at inlet which is comparable to the known VGJ investigations in literature [4, 10–13].

Numerical model

Only 25% of the span at the blade's mid-span region are modelled including three injection holes of each type (Fig 8).

TABLE 1. Mesh spacing in wall units at injection position, $Re_{2is} = 200 \cdot 10^3$, type I

	Δt^+	Δn^+	Δz^+
minimum	3.0	1.3	4.5
maximum	8.6	-	11.8

Hub and tip are treated with Euler boundary conditions. At the pitch boundaries translational periodicity is assumed. The VGJs are fully resolved in space including the injection holes and the secondary air system (plenum). The interface between the VGJ hole's and the blade's mesh is realized by zonal mixed interfaces (see [40]) whereas the grid density on both sides of the interface is similar. Grid independence of the results was achieved via a sensitivity study in the vicinity of the injection points (not shown here) leading to 1.9 million (type I) and 2.9 million grid points (type II). Hence, mesh spacings in the vicinity of the injection point as shown in Table 1 are attained. At the plenum inlets at hub and tip total pressure and flow direction boundary conditions are applied. Since the plenum's $Re_D < 1000$ its inlet flow is assumed to be laminar so that a turbulence intensity of 0.1%, $\gamma = 0$ and $Re_\Theta = f(Tu)$ are prescribed.

Results without VGJ Criterion

Prior to the discussion of the computations with VGJ it is reasonable to review TRACE's prediction quality of the T161 profile without VGJ. Figure 7 illustrates the non-dimensional pressure distributions c_p at mid-span for $Re_{2is} = 70 \cdot 10^3$ (left) and $200 \cdot 10^3$ (right). At both Re_{2is} the experimental values are captured nearly perfectly, only at $Re_{2is} = 70 \cdot 10^3$ the suction side's separation bubble is predicted slightly too short. The integral total pressure losses $\zeta_{V,m}$ (Fig. 6 right) also coincide very well with the experiments for the whole Re_{2is} range, whereas the wake itself, characterized by ζ_V, is predicted slightly too thin and intense (Fig. 6 left for $Re_{2is} = 200 \cdot 10^3$).

Looking at the c_p of the type I configuration at $B = 0.5$ and $Re_{2is} = 70 \cdot 10^3$ (Fig. 9) a good agreement of the experimental and computational results without VGJ transition mode (solid black line) can be observed - except the region downstream the injection position on the profile's suction side. Immediately downstream the VGJ between $x_{ax}/l_{ax} = 0.65 \ldots 0.85$ a too high c_p is predicted (1 in Fig. 9 right) whereas at the trailing edge 2 a too low value is computed. Both characteristics point to the false prediction of an open separation without reattachment (compare with upper part of Fig. 16). This conclusion is supported by the massively over estimated wake (Fig. 10 left) which is shifted to the direction of the suction side and the too high integral pressure loss $\zeta_{V,m}$ (Fig. 10 right). With regard to the lapse rate of the

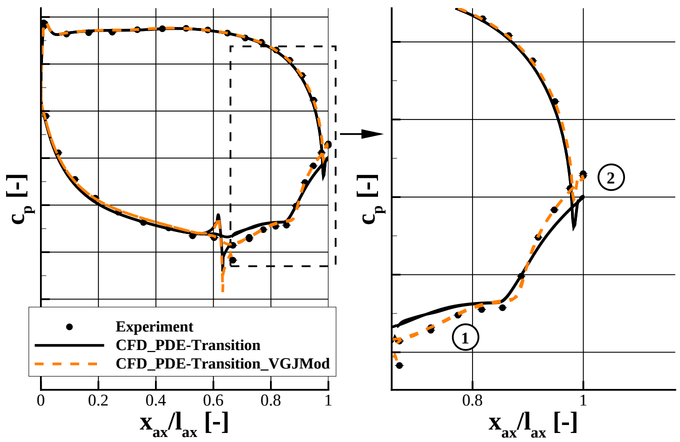

FIGURE 9. c_p of $Re_{2is} = 70 \cdot 10^3$, type I, $B = 0.5$ (left) and associated magnification of the trailing edge region (right)

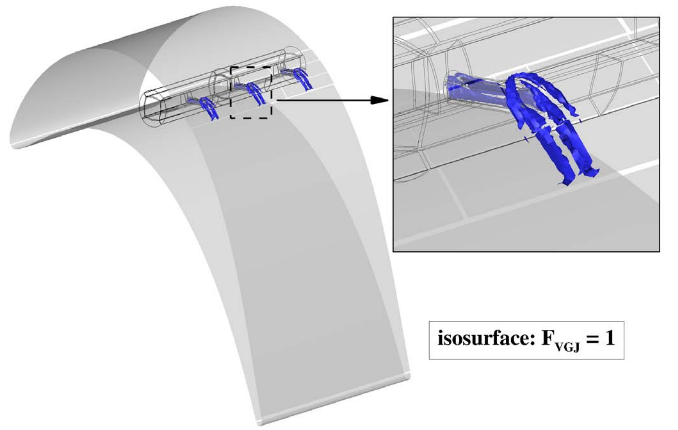

FIGURE 11. Isosurface $F_{VGJ} = 1$ at $Re_{2is} = 70 \cdot 10^3$, type I, $B = 0.5$ (geometry distorted)

losses through the whole Re_{2is} range the predicted loss increase is too large.

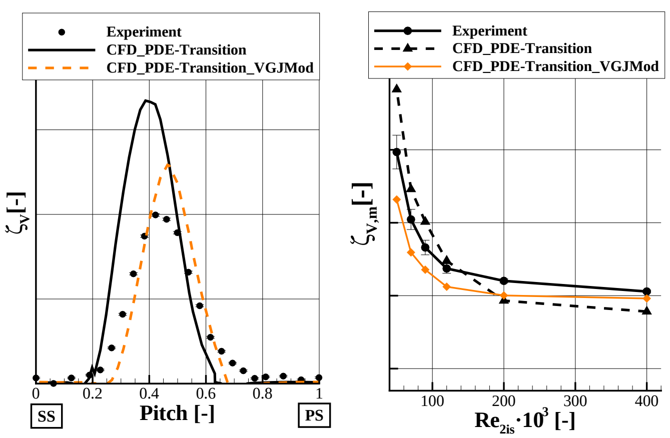

FIGURE 10. ζ_V of $Re_{2is} = 70 \cdot 10^3$ (left) and ζ_V, m for $Re_{2is} = 50 \cdot 10^3 ... 400 \cdot 10^3$ (right), type I, $B = 0.5$

This characteristic is also observed at a higher blowing ratio $B = 1.0$ (Fig. 12) and at the second injection position further downstream (type II) for two blowing ratios $B = 1.0$ (Fig. 13) and 1.5 (Fig. 14). In all cases the high losses are consistent to the c_p-distribution near the trailing edge, typical of non-reattaching boundary layers. The development of the eddy viscosity μ_t downstream the VGJ (Fig. 15 upper part) shows no impact of the three jets, turbulence production starts in conjunction with the massive separation. This leads to the conclusion that the production of eddy viscosity is insufficient and responsible for the non-reattaching boundary layer. These results with the γ-Re_{Θ} transition model fully agree with the investigations of Herbst et al. [15] with the *multimode transition* model without extra VGJ transition mode.

Results with VGJ Criterion

Figure 11 presents for one operating point the regions where the derived transition criterion F_{VGJ} leads to the application of the modified $P_{\Theta t,VGJ}$ (Eqn. 14). It can be seen that F_{VGJ} is equal 1 only in reasonable regions and that it clearly detects the dominant JICF vortical structures.

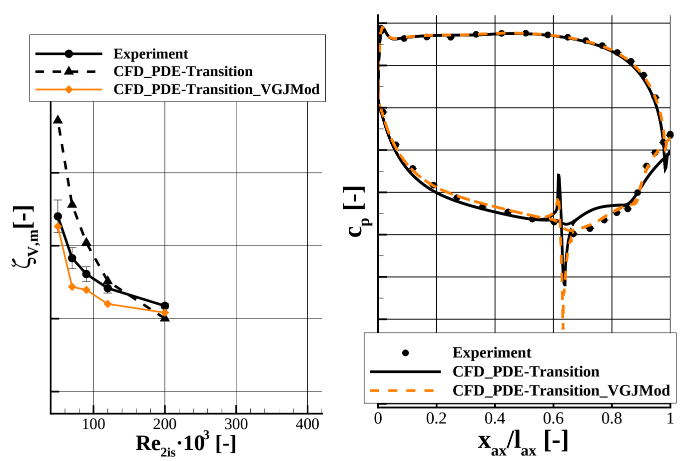

FIGURE 12. ζ_V, m for $Re_{2is} = 50 \cdot 10^3 ... 200 \cdot 10^3$ (left) and c_p of $Re_{2is} = 70 \cdot 10^3$ (right), type I, $B = 1.0$

At first applying the production term modification to the validation testcase with VGJ type I and $B = 0.5$ at $Re_{2is} = 70 \cdot 10^3$ a significant improvement of the prediction quality of all aerodynamic design parameters is apparent. The c_p distribution downstream the VGJ and especially at the trailing edge coincide very well with the experimental values (dashed orange line in Fig. 9) - the boundary layer reattaches upstream the trailing edge. This is accompanied by a reduction of the wake losses ζ_V leading to a good agreement with the experimental values similar to that of the cases without VGJ (e.g. Fig. 6 left). Furthermore, the computational integral losses $\zeta_{V,m}$ show qualitatively nearly the same lapse rate as the experimental, only a minor, almost constant shift to lower values is existing.

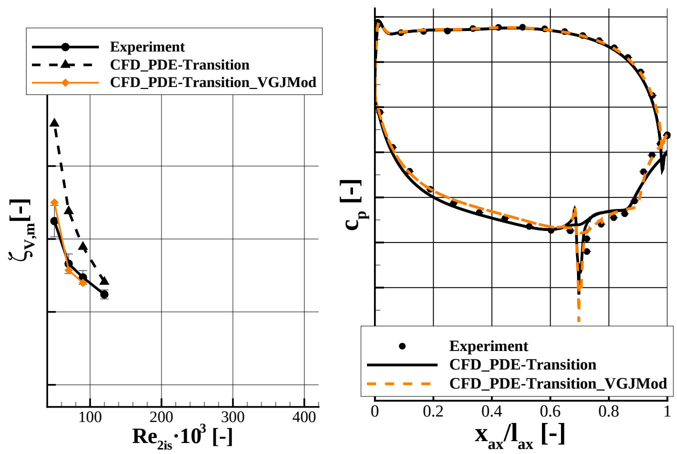

FIGURE 13. ζ_V,m for $Re_{2is} = 50 \cdot 10^3 ... 120 \cdot 10^3$ (left) and c_p of $Re_{2is} = 70 \cdot 10^3$ (right), type II, $B = 1.0$

A similar coincidence of $\zeta_{V,m}$ for the whole Re_{2is} range with the experiments can be observed for type I and $B = 1.0$ (Fig. 12) and an even better agreement for type II and $B = 1.0$ (Fig. 13). For both configurations the reduction of the losses compared to the unmodified transition model can be traced back to the (correct) reattachment of the boundary layer downstream the VGJ which again can be concluded with the help of the c_p distributions. Although the latter is also in good accordance with the experiments for the highest blowing ratio investigated here ($B = 1.5$ of the type II configuration) the integral total pressure loss $\zeta_{V,m}$ is computed about 28 per cent of the experimental value too low in this case (Fig. 14). Since the current first model version does not incorporate the blowing ratio as a correlation parameter in $P_{\Theta t,VGJ}$ future versions might take it into account. Especially as the VGJ's influence on transition was shown in literature [13] to be dependent on B.

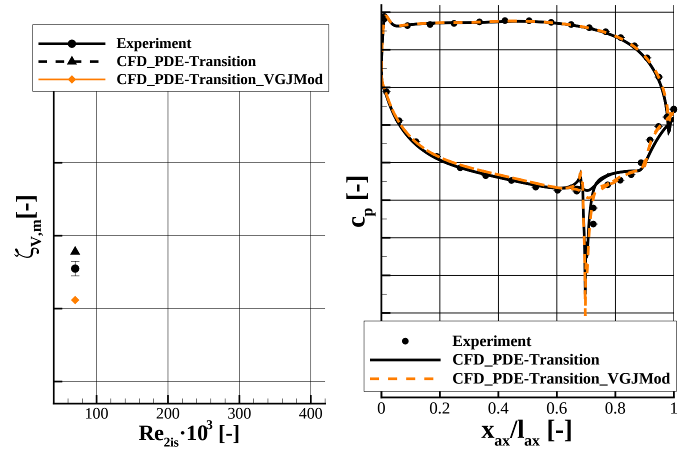

FIGURE 14. ζ_V,m (left) and c_p (right) at $Re_{2is} = 70 \cdot 10^3$, type II, $B = 1.5$

The models impact on the eddy viscosity level μ_t and therefore on the transition is illustrated in the lower part of Fig. 15. With regard to the DNS of Postl [13] a physical reasonable onset of transition (growth of μ_t) can be observed a certain distance downstream the injection position in a circular area. This area as well as the level of μ_t is increasing downstream whereas neighbouring jets do not interact. Further downstream μ_t is also growing in the spanwise direction in between the jets due to the development of a separation bubble (see lower part of Fig. 16). It is worth mentioning that the overall eddy viscosity level especially in the wake region is around 20% lower with the new model than with the unmodified transition model (Fig. 15 upper).

Finally, the separation reducing effect of the VGJ with the newly introduced model is shown in Fig. 16. In the computation without VGJ transiton mode a separation covers about 25% axial length of the suction side's aft part over the full span. By the discrete and slight increase of the turbulence level downstream the VGJ this separation is "cut" in spanwise pieces. By changing the structure of the separation not only a reattachment of the boundary layer directly downstream the VGJ is achieved but also in the spanwise regions in between.

CONCLUSIONS

A model for transition due to steady blowing vortex generating jets (VGJ) on high-lift low-pressure turbine profiles was introduced using a γ-Re_Θ transport-equation transition-model. Steady simulations were conducted using the turbomachinery research and design CFD code TRACE with the k-ω turbulence model.

By applying the Q vortex criterion in conjunction with the magnitude of the relative helicity, typical vortical structures in-

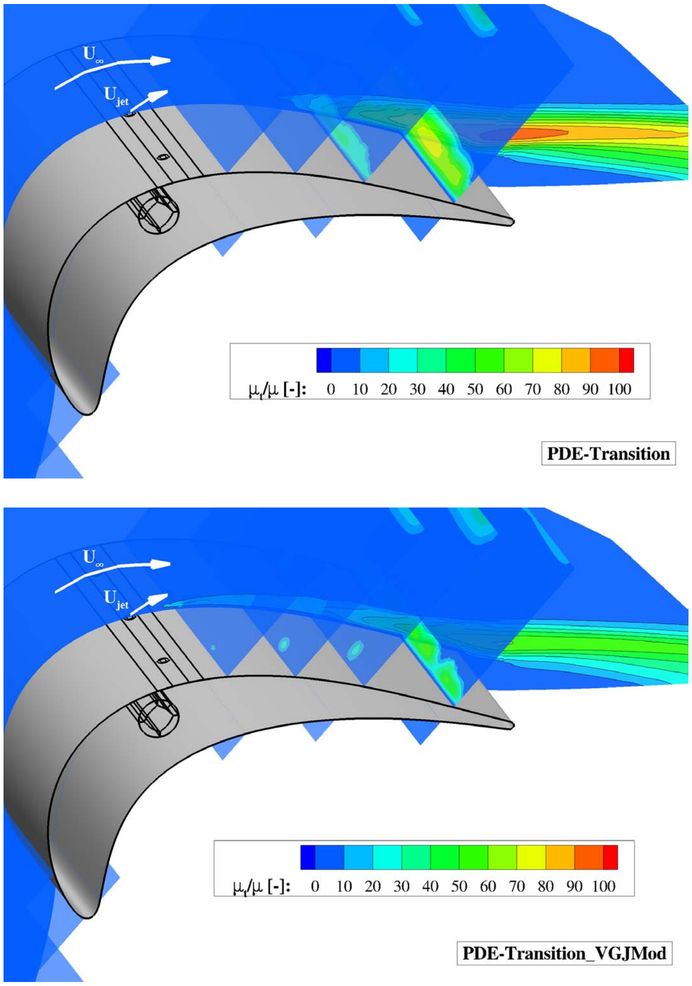

FIGURE 15. μ_t/μ downstream VGJ without (upper) and with (lower) VGJ transition mode, at $Re_{2is} = 70 \cdot 10^3$, type I, $B = 0.5$ (geometry distorted)

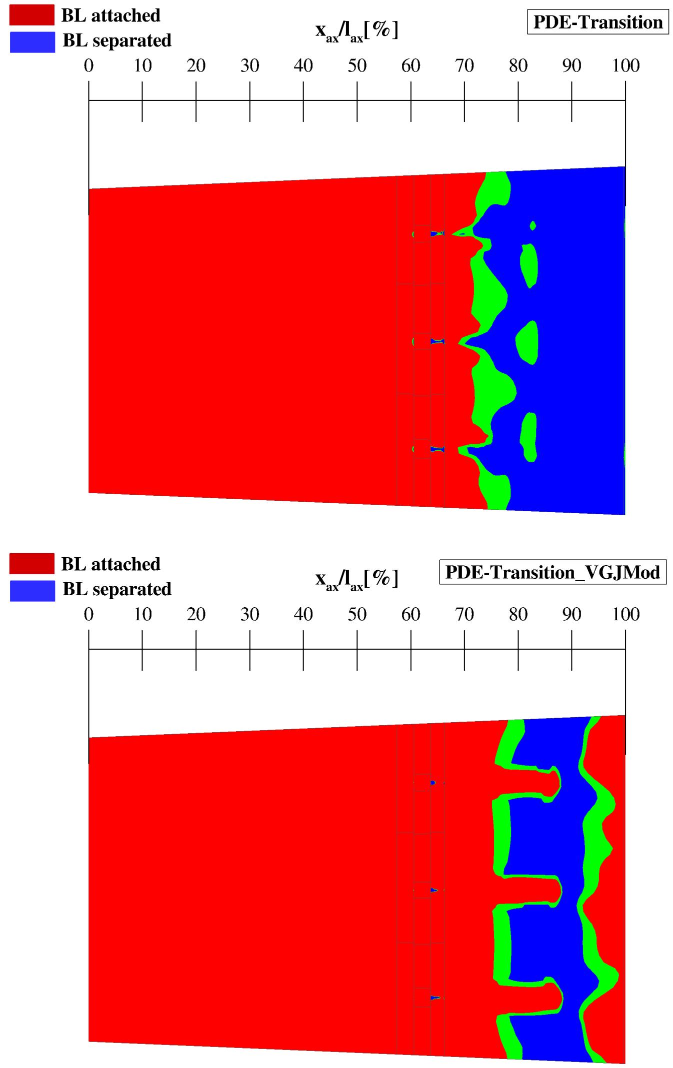

FIGURE 16. Boundary layer separation (derived form τ_w) at the profile's suction side without (upper) and with (lower) VGJ transition mode, at $Re_{2is} = 70 \cdot 10^3$, type I, $B = 0.5$

duced by VGJs were isolated in three-dimensional space. In these distinct regions, the transition process was modelled by massively reducing $\tilde{R}e_{\Theta t}$ by means of negative values of its production term.

The new model was validated against extensive cascade wind-tunnel experiments of a high-lift LPT profile at high-speed conditions for a wide range of Re_{2is}. Two different injection positions as well as three blowing ratios $B = 0.5, 1.0, 1.5$ were investigated.

Due to the new model, the local transition process was captured in accordance with the physics known from literature. Its application leads to a nearly perfect prediction of surface pressure distributions and to a very good reproduction of the total pressure losses. Compared to the original unmodified transition model, the new model, especially at Reynolds numbers $\leq 100 \cdot 10^3$, prevented the false prediction of lossy non-reattaching separation downstream the VGJs.

Since the prediction quality declined for higher blowing ratios, future versions of the VGJ transition mode will consider B as a correlation parameter. Furthermore, because the current work was limited to the blade's midspan region, the influence of real flow conditions including end wall effects on the model's behaviour will be investigated in the following work. Finally, the model will be applied to a complete turbine rig with VGJs (e.g. [14]).

ACKNOWLEDGMENT

The authors gratefully acknowledge the substantial contributions of the DLR Institute of Propulsion Technology, especially Dr. Edmund Kügeler, and MTU Aero Engines, namely Matthias Franke, Dr. Andreas Fiala and Dr. Karl Engel. We thank Prof. Reinhard Niehuis and Tom Ludewig of the University of the Armed Forces in Munich for the valuable discussions concerning the experimental results. Furthermore, the authors thank MTU Aero Engines for the permission to publish this work. The results presented in this paper have been obtained within *4th Aeronautical Research Program* of the German Ministry of Economics.

REFERENCES

[1] Hourmouziadis, J., 1989. "Aerodynamic Design of Low Pressure Turbines". AGARD Lecture Series 167.

[2] Mayle, R. E., 1991. "The Role of Laminar-Turbulent Transition in Gas Turbine Engines". *Journal of Turbomachinery,* ***113***(4), pp. 509–536.

[3] Gier, J., Franke, M., Hübner, N., and Schröder, T., 2008. "Designing LP Turbines for optimized Airfoil Lift". In Proceedings of ASME Turbo Expo, no. GT2008-51101.

[4] Bons, J. P., Sondergaard, R., and Rivir, R. B., 1999. "Control of low-pressure turbine separation using vortex generator jets". In 37th AIAA Aerospace Sciences Meeting and Exhibit, no. AIAA-99-0367.

[5] Gier, J., Raab, I., Schröder, T., Hübner, N., Franke, M., Kennepohl, F., Lippl, F., and Germain, T., 2007. "Preparation of Aero Technology for New Generation Aircraft Engine LP Turbines". In European Air and Space Conference, no. CEAS-2007-139.

[6] Volino, R. J., Kartuzova, O., and Ibrahim, M. B., 2009. "Experimental and Computational Investigations of Low-Pressure Turbine Separation Control using Vortex Generator Jets". In Proceedings of ASME Turbo Expo, no. GT-2009-59983.

[7] Gad El Hak, M., 2006. *Flow Control - Passive, Active and Reactive Flow Management*. Cambridge University Press, Cambridge.

[8] Lou, H., Qiao, W., and Xu, K., 2009. "Passive Control of Laminar Separation Bubble with Spanwise Groove on a Low-Speed Highly Loaded Low-Pressure Turbine Blade". *Journal of Thermal Science,* ***18***(3), pp. 193–201.

[9] Himmel, C. G., Thomas, R. L., and Hodson, H. P., 2009. "Effective Passive Flow Control for Ultra-Highlift Low Pressure Turbines". In Proceedings of 8th European Conference on Turbomachinery - EUROTURBO 8.

[10] Volino, R. J., 2003. "Passive Flow Control on Low-Pressure Turbine Airfoils". *Journal of Turbomachinery,* ***125***(4), pp. 754–764.

[11] McAuliffe, B. R., and Sjolander, S. A., 2004. "Active Flow Control Using Steady Blowing for a Low-Pressure Turbine Cascade". *Journal of Turbomachinery,* ***126***(4), pp. 560–569.

[12] McQuilling, M., and Jacob, J., 2004. "Effect of Chord Location on Separation Control with Vortex Generator Jets on Low Pressure Turbine Blades". In 2nd Flow Control Conference, no. AIAA 2004-2205.

[13] Postl, D., 2005. "Numerical investigation of laminar separation control using vortex generating jets". PhD thesis, Department of Aerospace and Mechanical Engineering, University of Arizona, Tucson.

[14] Schumann, T., Rose, M. G., Staudacher, S., Gier, J., and Schröder, T., 2008. "The Effects of Steady Injection on an Ultra High Lift Vane in a LP Turbine". In Proceedings of ASME Turbo Expo, no. GT2008-50330.

[15] Herbst, F., Biester, M., Fiala, A., Engel, K., and Seume, J. R., 2010. "Validation of RANS-Modelling Approaches for Active Flow Control by Vortex Generating Jets in a Low-Pressure Turbine Cascade". In Proceedings of the 8th International Symposium on Engineering Turbulence Modelling and Measurements - ETMM8.

[16] Volino, R. J., 2003. "Separation control on low-pressure turbine airfoils using synthtic jet vortex generator jets". *Journal of Turbomachinery,* ***125***(4), pp. 765–777.

[17] Margason, R. J., 1993. "Fifty Years of Jet in Crossflow Research". In AGARD, Computational and Experimental Assessment of Jets in Cross Flow, Nangia, R. K., ed.

[18] Compton, D. A., and Johnston, J. P., 1992. "Streamwise Vortex Production by Pitched and Skewed Jets in a Turbulent Boundary Layer". *AIAA Journal,* ***30***(3), pp. 640–647.

[19] McGovern, K. T., and Leylek, J. H., 2000. "A Detailed Analysis of Film Cooling Physics: Part II - Compound-Angle Injection with Cylindrical Holes". *Journal of Turbomachinery,* ***122***(1), pp. 113–121.

[20] Sondergaard, R., Rivir, R. B., and Bons, J. P., 2002. "Control of low-pressure turbine separation using vortex-generator jets". *Journal of Propulsion and Power,* ***18***(4), pp. 889–895.

[21] Eldredge, R., and Bons, J., 2004. "Active control of a separating boundary layer with steady vortex generating jets -detailed flow measurements". In 42nd AIAA Aerospace Sciences Meeting and Exhibit, no. AIAA 2004-751.

[22] Rizzetta, D. P., and Miguel, R. V., 2006. "Numerical Study of Active Flow Control for a Transitional Highly Loaded Low-Pressure Turbine". *Journal of Fluids Engineering,* ***128***(5), pp. 956–966.

[23] Postl, D., Gross, A., and Fasel, H. F., 2004. "Numerical Investigation of Active Flow Control for Low-Pressure Turbine Blade separation". In 42nd AIAA Aerospace Sciences Meeting and Exhibit, no. AIAA 2004-0750.

[24] Garg, V. K., 2002. "Low-Pressure Turbine Separation Control - Comparison with Experimental Data". In Proceedings of ASME Turbo Expo, no. GT-2002-30229.

[25] Rumsey, C. L., and Swanson, R. C., 2009. "Turbulence modelling for active flow control application". *International Journal of Computational Fluid Dynamics,* ***23***(4), pp. 317–326.

[26] Kožulović, D., Röber, T., and Nürnberger, D., 2007. "Application of a Multimode Transition Model to Turbomachinery Flows". In Proceedings 7th European Turbomachinery Conference.

[27] Langtry, R., and Menter, F., 2009. "Correlation-Based Transition Modeling for Unstructured Parallelized Computational Fluid Dynamics Codes". *AIAA Journal,* ***47***(12), pp. 2894–2906.

[28] Marciniak, V., Kügeler, E., and Franke, M., 2010. "Predicting Transition on Low-Pressure Turbine Profiles". In Proceedings V European Conference on Computational Fluid Dynamics ECCOMAS CFD 2010.

[29] Kügeler, E., Nürnberger, D., Weber, A., and Engel, K., 2008. "Influence of blade fillets on the performance of a 15 stage gas turbine compressor". In Proceedings of ASME Turbo Expo, no. GT2008-51101.

[30] Yang, H., Nuernberger, D., and Kersken, H.-P., 2006. "Toward excellence in turbomachinery computational fluid dynamics: A hybrid structured-unstructured reynolds-averaged navier-stokes solver". *Journal of Turbomachinery,* ***128***(2), pp. 390–402.

[31] Wilcox, D. C., 2006. *Turbulence Modelling for CFD*, third ed. DCW Industries.

[32] Röber, T., Kožulović, D., Kügeler, E., and Nürnberger, D., 2006. "Appropriate Turbulence Modelling for Turbomachinery using a Two-equation Turbulence Model". In *New Results in Numerical and Experimental Fluid Mechanics V*, H.-J. Rath, C. Holze, H.-J. Heinemann, R. Henke, and H. Hnlinger, eds., Vol. 92 of *Notes on Numerical Fluid Mechanics and Multidisciplinary Design*. Springer Berlin / Heidelberg, pp. 446–454.

[33] Malan, P., Suluksna, K., and Juntasaro, E., 2009. "Calibrating the γ-Re_Θ Transition Model". *ERCOFTAC Bulletin,* ***80***, pp. 53–57.

[34] Jeong, J., and Hussain, F., 1995. "On the identification of a vortex". *Journal of Fluid Mechanics,* ***285***.

[35] Hunt, J. C. R., Wray, A. A., and Moin, P., 1988. "Eddies, streams, and convergence zones in turbulent flows". In Proceedings of the 1988 Summer Program, pp. 193–208.

[36] Lengani, D., Simoni, D., Ubaldi, M., Zunino, P., and Bertini, F., 2009. "An Experimental Study of the Reynolds Number Influence on a Laminar Separation Bubble". *ERCOFTAC Bulletin,* ***80***, pp. 24–28.

[37] Kožulović, D., and Röber, T., 2006. "Modelling the streamline curvature effects in turbomachinery flows". In Proceedings of ASME Turbo Expo, no. GT2008-51101.

[38] Ludewig, T., and Niehuis, R., 2008. Untersuchungen am Turbinengitter T161-T-Jet mit saugseitiger Ausblasung zur Bestimmung des Grenzschichtverhaltens, Abschlussbericht zum Messprogramm 216. Forschungsbericht der Universität der Bundeswehr München, Unpublished Internal Report MTU Aero Engines.

[39] Amecke, J., 1967. Auswertung von Nachlaufmessungen an ebenen Schaufelgittern. Tech. Rep. Bericht 67 A 49, AVA Göttingen.

[40] Yang, H., Nuernberger, D., Nicke, E., and Weber, A., 2003. "Numerical investigation of casing treatment mechanisms with a conservative mixed-cell approach". In Proceedings of ASME Turbo Expo, no. GT-2003-38483.